

Evidence from gravity anomalies for interactions of the Marion and Bouvet hotspots with the Southwest Indian Ridge: effects of transform offsets

Jennifer E. Georgen^{a,*}, Jian Lin^b, Henry J.B. Dick^b

^a MIT-WHOI Joint Program in Oceanography, Woods Hole Oceanographic Institution, Woods Hole, MA 02543, USA

^b Department of Geology and Geophysics, Woods Hole Oceanographic Institution, Woods Hole, MA 02543, USA

Received 15 July 2000; received in revised form 13 February 2001; accepted 23 February 2001

Abstract

The ultra-slow spreading Southwest Indian Ridge (SWIR) presents a unique environment to study the interactions between hotspots and ridges with highly segmented geometry. Using recently available satellite free-air gravity and shipboard bathymetry data, we obtain mantle Bouguer (MBA) and residual mantle Bouguer anomalies (RMBA) by removing from free-air gravity the attractions of seafloor topography, sediment thickness variations, a reference crust, and theoretically predicted effects of lithospheric cooling. The Bouvet hotspot, previously observed to be associated with anomalous bathymetry and geochemistry near the Bouvet triple junction, has an MBA axial gravity low of ~ 100 mGal, implying pronounced localized crustal thickening. Off-axis, the RMBA lows along previously calculated Bouvet hotspot tracks are variable in amplitude, suggesting the possibilities that Bouvet flux varies in time or that hotspot magmatism is enhanced by proximity to a spreading center. Along-axis geophysical anomalies suggest that the Marion hotspot has a significant effect on accretionary processes in the central portion of the SWIR. Importantly, the Marion axial anomaly appears to be compartmentalized between the Andrew Bain and Discovery II fracture zones, implying that transform offsets play a significant role in governing the distribution of plume material in a highly segmented, ultra-slow spreading system. © 2001 Elsevier Science B.V. All rights reserved.

Keywords: Bouguer anomalies; hot spots; Southwest Indian Ridge; transform faults; mid-ocean ridges

1. Introduction

The accretion of oceanic crust along the global

mid-ocean ridge system is influenced greatly by the presence of nearby mantle plumes. Most studies of ridge-hotspot interactions have focused on the Atlantic and eastern Pacific ocean basins, where relatively abundant data are available. In contrast, comparatively poor coverage of conventional underway geophysical data has hindered the investigation of hotspots in the southern oceans. Recently released satellite-derived gravity [1], however, permits the inclusion of southern ocean hotspots in global studies of plume-ridge

* Corresponding author. Tel.: +1-508-289-2581;
Fax: +1-508-457-2187; E-mail: jgeorgen@mit.edu
E-mail: jlin@whoi.edu
E-mail: hdick@whoi.edu

interaction. Moreover, recent compilation of the GEBCO digital database [2] represents a major improvement in bathymetric data coverage in the southern oceans. This study combines ship-track bathymetry and satellite gravity to determine gravity anomalies for the western Indian and southern Atlantic oceans. We use mantle Bouguer anomaly (MBA) and residual MBA (RMBA) to characterize the interactions of the Marion and Bouvet hotspots with the Southwest Indian Ridge (SWIR) and to provide constraint for Marion and Bouvet hotspot tracks. Further, we place Marion and Bouvet in a global context by comparing them with other spreading center–plume systems, and consider the important role of transform faults in plume–ridge interactions at this ultra-slow spreading rate.

2. Geological setting

The SWIR extends ~ 8000 km from the Bouvet triple junction (BTJ) in the west to the Rodrigues triple junction (RTJ) in the east (Fig. 1). The SWIR is among the world's slowest spreading ridges, with a full spreading rate close to ~ 13 – 16 mm/yr along most of its length. Marion Island, which is located on 28 Ma crust about 250 km from the SWIR [3], marks the current position of the Marion/Prince Edward plume (hereafter referred to as the Marion plume) [4,5]. Bouvet Island lies on 7 Ma crust [3], approximately 300 km to the east of the BTJ and 55 km from the nearest segment of the SWIR. Several recent papers have investigated whether Bouvet Island or Spiess Seamount, located between the BTJ and Bouvet Island, is the position of the Bouvet plume (e.g. [6–8]). However, this question has not yet been resolved, so we will place the plume at Bouvet Island unless otherwise noted.

The configuration of the SWIR varies significantly along its strike, and the ridge may be divided into a number of subsections based on geometry and spreading history (Fig. 1). The first subsection extends from the BTJ to 10°E and is characterized by short ridge segments and closely spaced transforms. This geometry is more or less mirrored by conjugate sections on the eastern

American–Antarctic Ridge (AAR). The second subsection consists of a 400-km-long length of ridge between 10°E and 15°E . This stretch lies at an oblique angle to the regional spreading direction, resulting in a confused segmentation pattern and very low effective spreading rate. The third subsection, between 15°E and 25°E , was the focus of a detailed geophysical survey by Grindlay et al. [9] where SeaBeam multibeam bathymetry, magnetics, and gravity data revealed that the ridge consists of a series of short (~ 45 km) segments separated by non-transform offsets. The 720-km-long Andrew Bain FZ and 150-km-long Du Toit FZ, which were also studied in the survey of Grindlay et al. [10], significantly displace the trend of the SWIR and constitute a fourth subsection. Between the Marion and Gallieni FZs, the fifth subsection, axial depth is relatively shallow and the segmentation pattern is somewhat irregular. In contrast, offsets between the Gallieni and Atlantis II FZs, subsection six, may be traced considerable distances off-axis in the satellite gravity map (Fig. 1). Subsection seven, the portion of ridge between Melville FZ and the RTJ, is characterized by marked obliquity accommodated by second-order segmentation, and has been created since 45 Ma by eastward migration of the RTJ [11]. An increase in axial depth from 49°E to the RTJ, as well as a relative lack of fresh volcanic activity as seen in TOBI sidescan sonar images, likely reflects amagmatic extension [12–14].

The highly segmented nature of the SWIR in the vicinity of Marion and Bouvet provides a unique opportunity to explore plume–ridge interactions at an ultra-slow spreading ridge. Prior studies of plume–ridge interactions have often focused on systems with relatively straight ridges. For example, both the Galapagos/Cocos–Nazca spreading center (CNSC) and the Iceland/Reykjanes Ridge systems have been extensively modeled (e.g. [15–19]), yet the CNSC is offset by only a few major (> 50 km) discontinuities near the Galapagos plume (e.g. [20]), and the Reykjanes Ridge south of Iceland is characterized by en echelon segments [21]. Long offsets in the SWIR such as the Andrew Bain FZ may exert important control on the dispersal of the Marion plume.

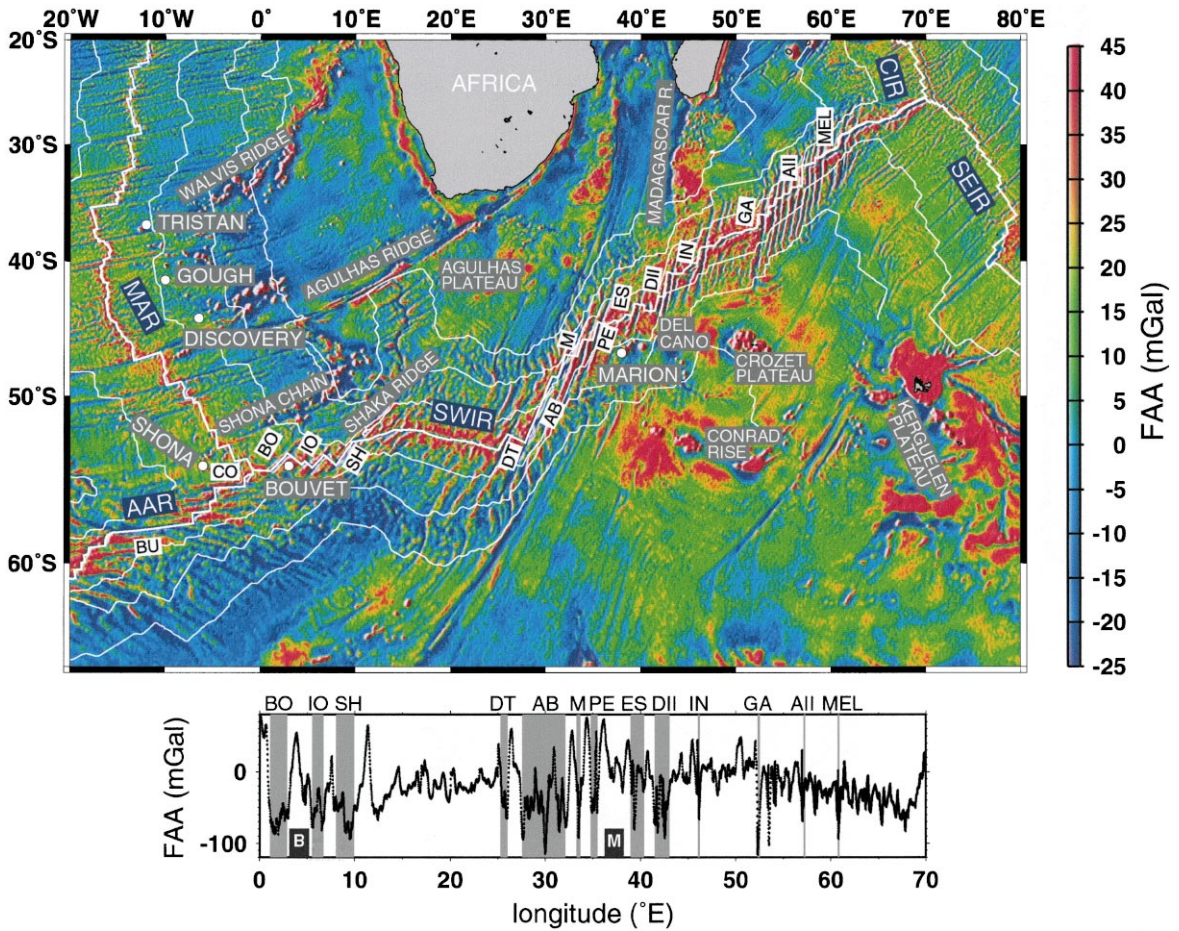


Fig. 1. Regional FAA map for the SWIR and part of the Southern Atlantic Ocean (data from [1]). Thick white lines mark the location of ridge axes: SWIR = Southwest Indian Ridge, SEIR = Southeast Indian Ridge, CIR = Central Indian Ridge, MAR = Mid-Atlantic Ridge, AAR = American–Antarctic Ridge. Locations of significant seafloor features are labeled in white lettering; positions of hotspots are marked with filled white circles. The names of prominent fracture zones are labeled as BU = Bullard FZ, CO = Conrad FZ, BO = Bouvet FZ, IO = Islas Orcadas FZ, SH = Shaka FZ, DT = Du Toit FZ, AB = Andrew Bain FZ, M = Marion FZ, PE = Prince Edward FZ, ES = Eric Simpson FZ, DII = Discovery II FZ, IN = Indomed FZ, GA = Gallieni FZ, AII = Atlantis II FZ, and MEL = Melville FZ. Thin white lines are 25, 50, and 75 Ma isochrons [3]. Gravity data are plotted at 5' spacing and an artificial illumination has been imposed on the grid from the NW. Lower panel shows FAA along the axis of the SWIR. Regions covering fracture zones are shaded, and the positions of the Marion and Bouvet hotspots are indicated with M and B, respectively.

3. Gravity analysis

3.1. Data sources

The primary bathymetry data source of this study was the recently released GEBCO digital database [2,22]. The GEBCO-97 database offers the position of bathymetric contours with depth values spaced at an interval of ~1–2 km along

the contours, which we projected onto a 5' grid (Fig. 2). The GEBCO-97 dataset, a compilation of accumulated shiptrack data from many sources, represents a major improvement in data coverage over any previous bathymetric database of the southern oceans. Note that shiptrack coverage is relatively dense along the ridge axis, especially near Marion and Bouvet islands (Fig. 2). To guard against overinterpretation of the GEBCO

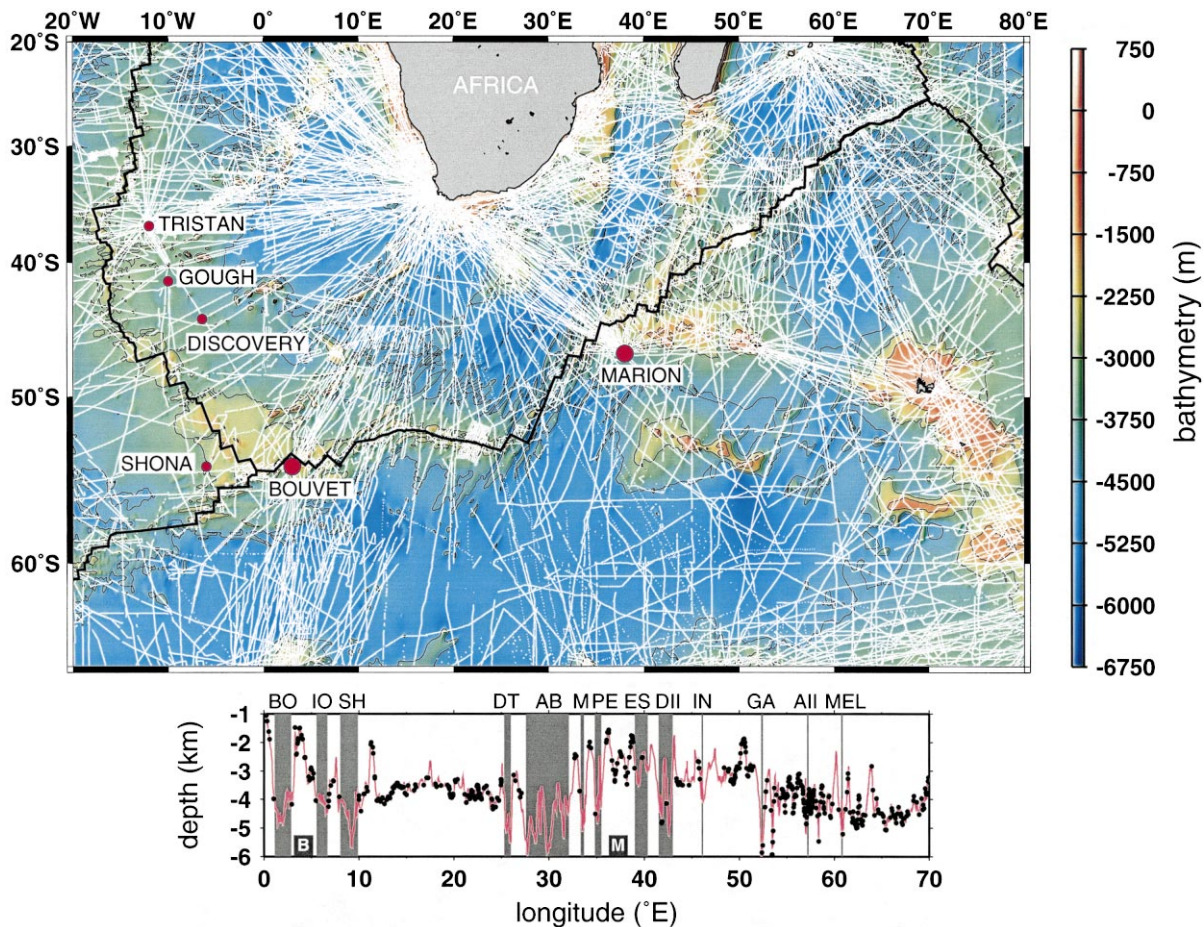


Fig. 2. Bathymetry map for the southwest Indian Ocean based on the GEBCO-97 database [2]. Thin white lines indicate ship-track coverage of the bathymetry data in the GEBCO-97 compilation, and red dots mark the locations of hotspots. Grid spacing is $5'$, contour interval is 1500 m, and artificial illumination is from the NW. Lower panel shows SWIR axial bathymetry (pink line). Depths constrained by shiptrack lines crossing spreading segments are indicated with black dots, regions covering fracture zones are shaded, and fracture zones and hotspots are labeled as in Fig. 1.

dataset, maps of gravity anomalies calculated using the GEBCO data (e.g. Figs. 3 and 5) were also projected on a $5'$ grid and all nodes lacking ship-track control within a $15'$ radius were masked.

We extracted free-air anomaly (FAA) gravity data from the $2'$ grid spacing global database calculated by Sandwell and Smith [1] from declassified Geosat and ERS-1 altimetry (Fig. 1). Neumann et al. [23] showed that the $3'$ grid that preceded the current $2'$ database is coherent with bathymetry to wavelengths as short as 27.5 km for the Mid-Atlantic Ridge between 31° and 36° S. Similarly, Rommevaux-Jestin et al. [12]

found reasonably good correspondence between shipboard and satellite FAA for wavelengths greater than 30–50 km for the eastern SWIR. We analyze this further below.

Sediment thickness data were extracted from a preliminary global database comprising digitized isopach maps gridded with $5'$ spacing [24]. Sediment thickness is less than 1000 m for most of the region. Maximum thicknesses occur within 5° of the African margin (5000 m) and in the southeastern portion of Fig. 2, east of 50° E and south of 60° S (4000 m).

We used the digital age grid of Mueller et al. [3]

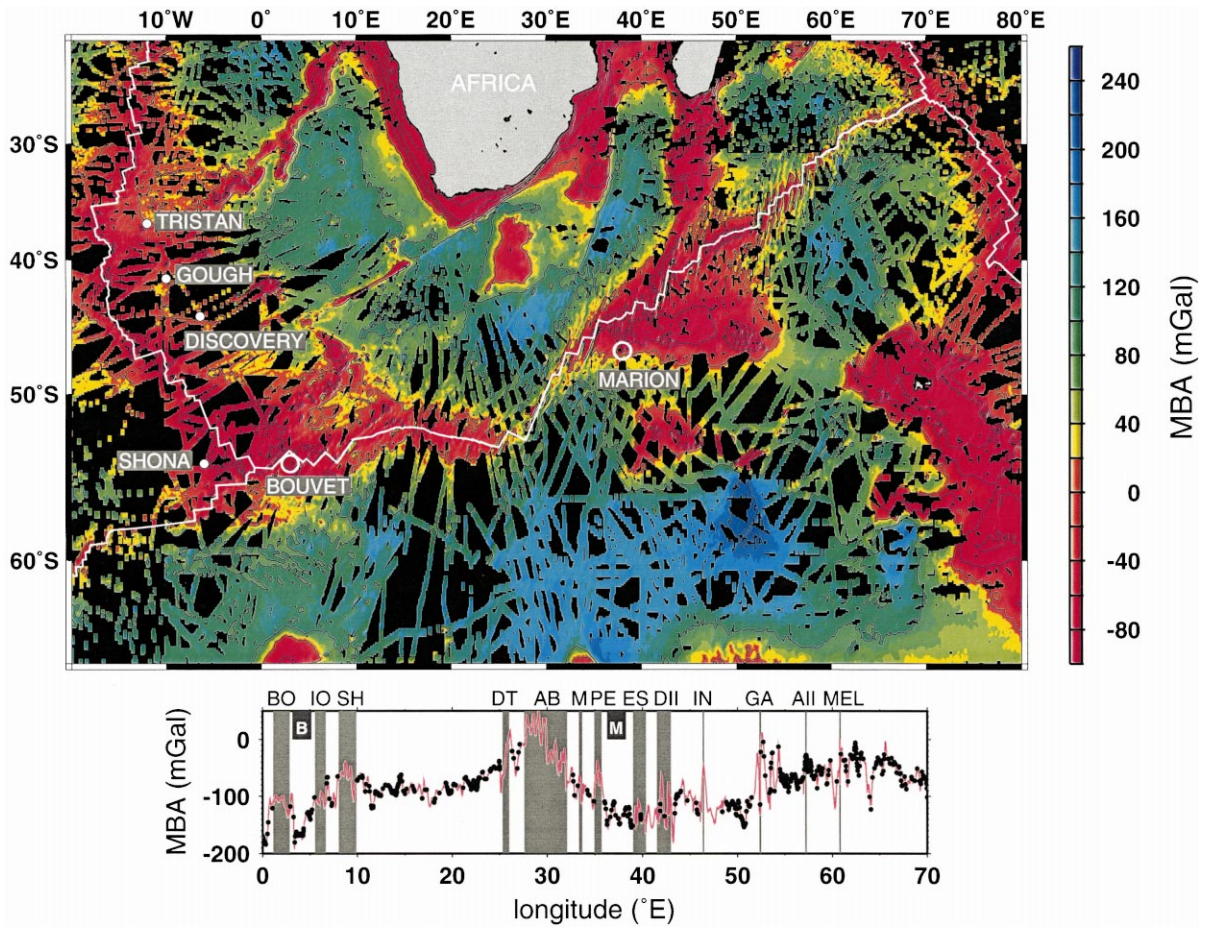


Fig. 3. Map of MBA, calculated by subtracting from FAA the gravitational effects of the water–sediment, sediment–crust, and crust–mantle interfaces assuming a constant 5-km-thick reference crust. The densities for seawater, sediment, crust, and mantle are assumed to be 1030, 2300, 2800, and 3300 kg/m³, respectively. Grid nodes without shiptrack control within a 15' radius are masked with black. Grid spacing is 5' and contour interval is 100 mGal. Artificial illumination is imposed from the NW. Lower panel shows MBA along the axis of the SWIR (pink line). MBA values constrained by shiptrack crossings of the ridge are indicated with black dots, regions covering fracture zones are shaded, and fracture zones and hotspots are labeled as in Fig. 1.

for gravity thermal corrections (Fig. 1). Age error estimations for more than two-thirds of the seafloor in the area of study are < 3 Myr [3]. Errors of such magnitude would have little effect on the calculated thermal correction for RMBA, described below. For young (< 25 Ma) crust, age errors of up to 5–8 Ma occur in isolated areas [3], such as the Bouvet FZ, the oblique section of ridge between 10°E and 15°E, and the Du Toit FZ. Such errors would translate to approximately 20 mGal in the RMBA thermal correction. Off-axis (> 25 Ma), large errors (> 8 Ma)

are also associated with the seafloor around the Shona Chain and between the Shona Chain and Shaka Ridge [3]. Such crustal age errors could correspond to RMBA thermal correction errors of up to 25 mGal.

3.2. Data analysis

The free-air gravity map shown in Fig. 1 contains signals from seafloor topography, sediments, and crust and mantle density anomalies. To reveal the more subtle crust and mantle anomalies, we

subtracted from FAA the theoretical gravity effects of the water–sediment, sediment–crust, and crust–mantle interfaces assuming a constant density 5-km-thick model crust. The densities for sea-water, sediment, crust, and mantle were assumed to be 1030, 2300, 2800, and 3300 kg/m³, respectively. The resulting MBA map is shown in Fig. 3.

The results of our MBA calculations are compared with those of the detailed geophysical survey of Grindlay et al. [9] along the SWIR axis

between 15.5°E and 25°E (Fig. 4a). The MBA results of Grindlay et al. [9] were obtained using high-resolution multibeam bathymetry and ship-board gravity data that were collected in early 1996 and were not included in the GEBCO-97 database. Although differing in detail, the two studies yield intermediate- to long-wavelength trends that are very similar (Fig. 4a). To quantify this similarity, we applied lowpass filters with varying cutoff wavelengths to both profiles and

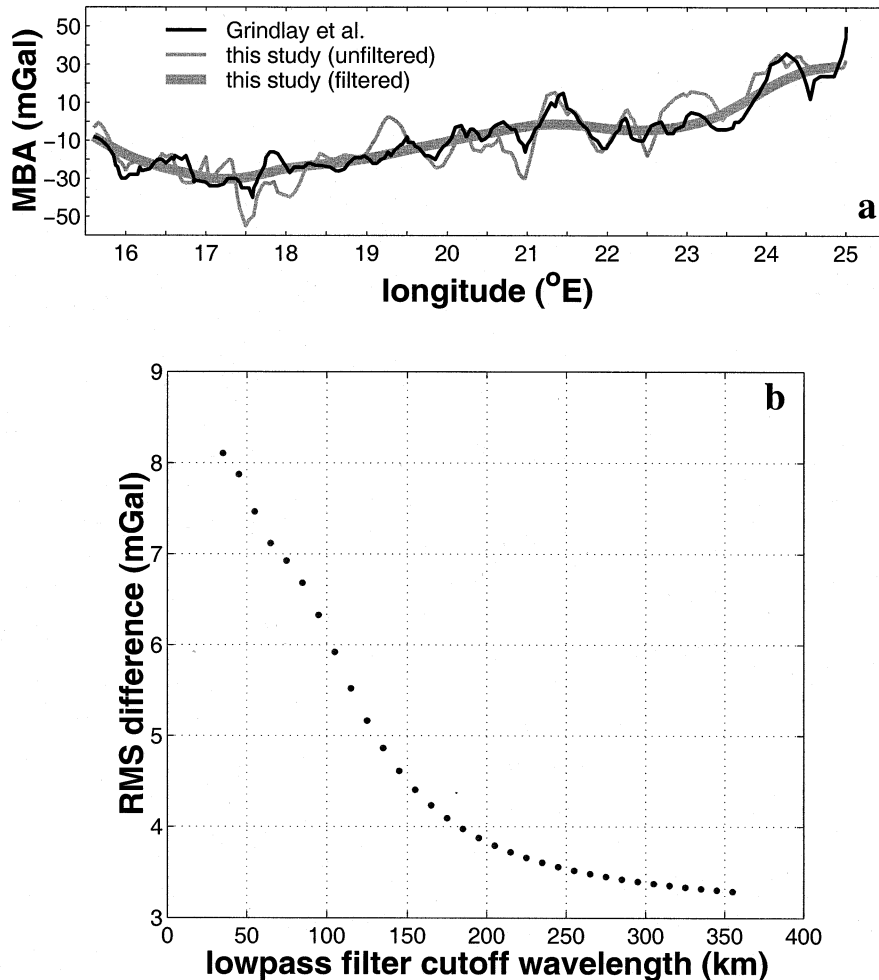


Fig. 4. (a) Comparison of axial MBA profiles for 15.5°E–25°E between the results of Grindlay et al. [9] and this study. Filtered profile is generated by applying 125-km cutoff lowpass filter to axial data sampled every 10 km. Note the general long-wavelength agreement between the two profiles despite differences in detail. (b) RMS difference between lowpass-filtered profiles from Grindlay et al. [9] and this study as a function of lowpass cutoff wavelength. Differences were taken every 10 km along the profile and filtered used a Hanning window.

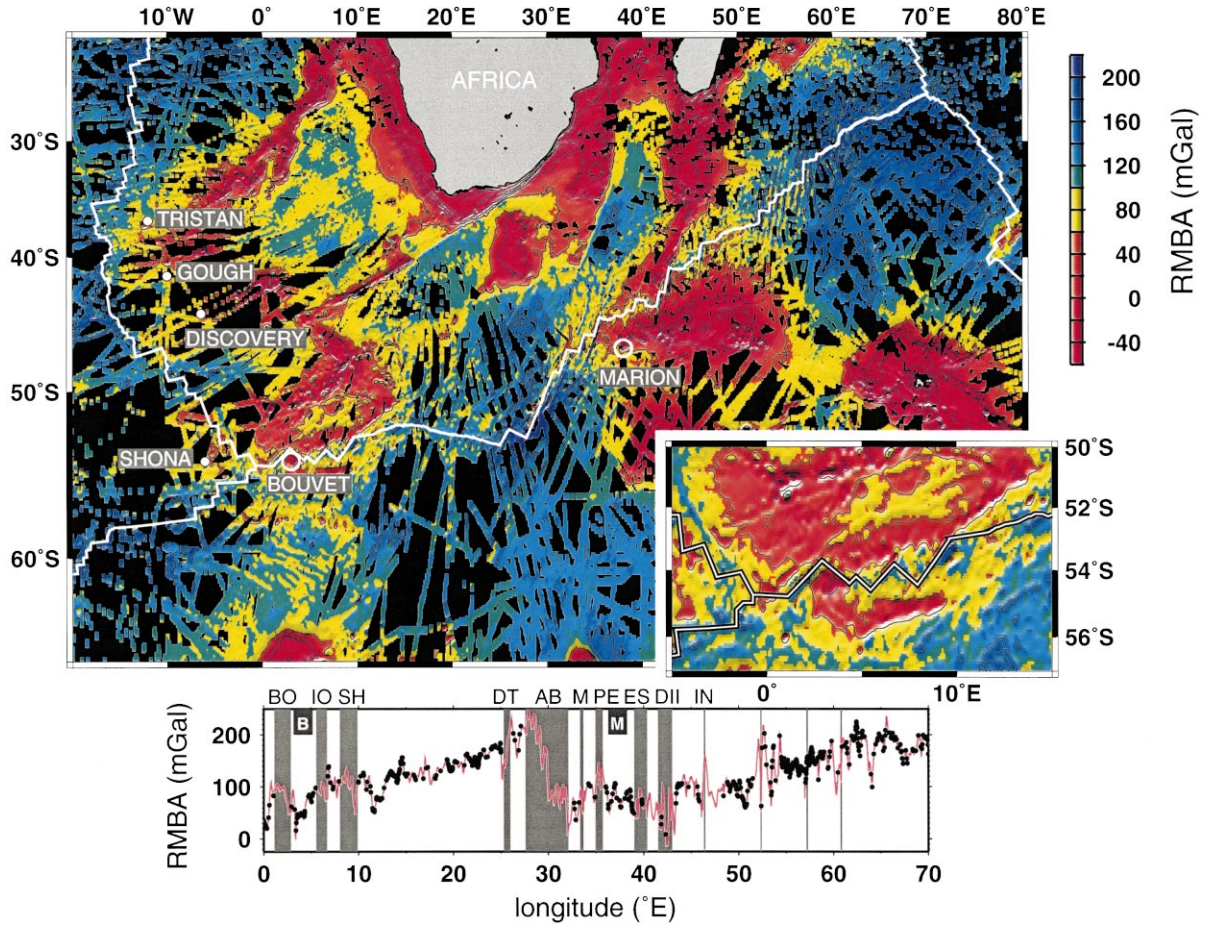


Fig. 5. Map of RMBA, created by subtracting from MBA the effects of lithospheric cooling based on an age-correction model. Masking is the same as in Fig. 3. Artificial illumination is imposed from the NW. Grid spacing is 5' and contour interval is 100 mGal. Inset shows RMBA in the immediate vicinity of the BTJ, without shiptrack masking. The lower panel displays along-axis RMBA (pink line) with RMBA values constrained by shiptrack crossings of the SWIR shown in black dots. Regions covering fracture zones are shaded and fracture zones and hotspots are labeled as in Fig. 1.

determined the root-mean-square (RMS) difference between the filtered data (Fig. 4b). The RMS difference decreases quickly with cutoff wavelength, reaching a value of approximately 5 mGal for a cutoff wavelength of 125 km. This suggests that intermediate- to long-wavelength features, such as hotspot swells, are resolved reasonably accurately in the present study.

The second step in gravity data reduction was removal of the effects of lithospheric cooling. We calculated a three-dimensional (3D) mantle temperature field based on crustal age from the Mueller et al. [3] database. For computational ease,

the plate cooling model [25] with temperature of 1350°C at the base of a 100-km lithosphere was used for crustal ages > 1 Ma, while the half-space solution [26] was employed for ages < 1 Ma. The gravity signals of this 3D mantle temperature field were then calculated and integrated down to 100 km depth to yield a theoretical estimation of the contribution of 3D lithospheric cooling to MBA (e.g. [27,28]), assuming a coefficient of thermal expansion of $3.5 \times 10^{-5} \text{ K}^{-1}$. An along-axis profile of the age-based thermal correction is shown in Fig. 6a. Subtraction of lithospheric cooling from MBA yielded RMBA (Fig. 5). RMBA re-

flects deviations in crustal structure and/or mantle temperature from the reference model. Areas with low RMBA may result from the combined effects of thicker crust, lower density crust, and/or higher temperature mantle than surrounding regions.

The Phipps Morgan and Forsyth [29] model, which calculates mantle flow patterns based on

ridge-transform geometry, was not used to determine the thermal correction for several reasons. First, unlike the age-based approach, the Phipps Morgan and Forsyth [29] model requires constant spreading rate both along the ridge and over time, which is an assumption clearly violated here given the large area under consideration. Also, the crus-

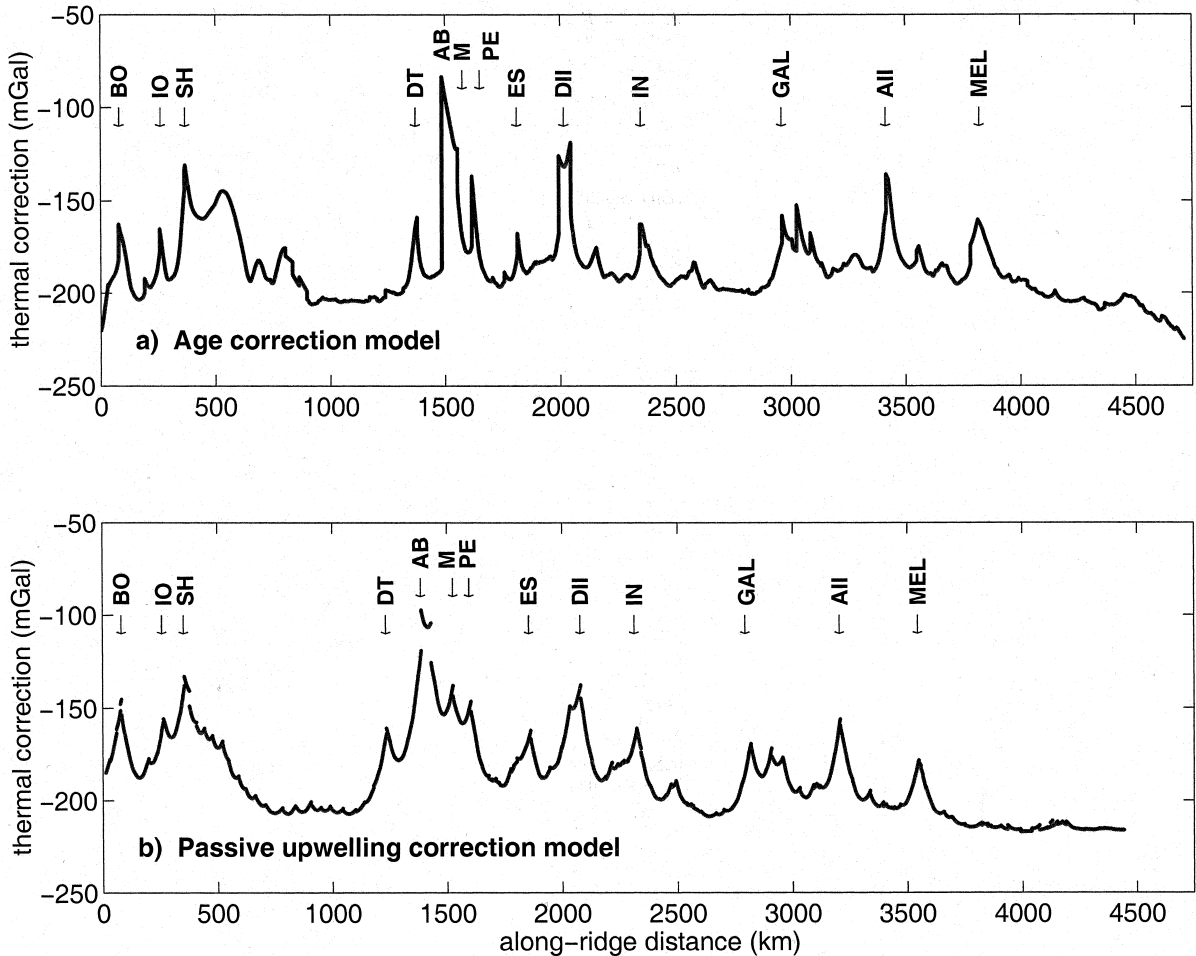


Fig. 6. Along-axis profiles of gravity thermal corrections calculated using (a) the age model and (b) the passive upwelling model. The age method assumes thermal cooling based on crustal age [3]. Mantle flow patterns in the passive upwelling model are calculated based on ridge-transform geometry, following [29]. The thermal structure resulting from the calculated 3D mantle flow field is then translated into density, assuming a coefficient of thermal expansion of $3.4 \times 10^{-5} \text{ K}^{-1}$. Finally, the FFT technique of Parker [45] is used to calculate gravity. The discrepancy in length between the two profiles results from orthogonalizing SWIR ridge segments and transforms before input into the passive upwelling code, a requirement of the Phipps Morgan and Forsyth [29] technique. Because the passive upwelling method takes into account the 3D nature of flow around transform faults, its predicted thermal corrections near long-offset transforms are broader than those calculated by the age method. However, the age method is more appropriate for the large area addressed by this study because it allows for non-constant spreading rates and can determine the gravity signal around a triple junction.

tal age method permits calculation of the 3D thermal structure for the BTJ and RTJ, which have more complex geometry than that allowed by the Phipps Morgan and Forsyth [29] approach. The use of crustal age rather than passive flow modeling for the calculation of thermal correction, however, may lead to an underestimation of the thermal effects associated with large fracture zones such as the Andrew Bain FZ, because the effects of reduced upwelling and lateral asthenospheric flow were not considered. For example, Fig. 6 shows thermal corrections calculated using both the age and passive upwelling approaches. The age-based method yields corrections that are much more localized around individual offsets, rather than the broader correction of the passive upwelling model. This effect is particularly pronounced for the closely spaced transforms around the Andrew Bain FZ. However, the maximum values of the thermal corrections at the Andrew Bain FZ are similar in the two models (Fig. 6).

4. Regional and along-axis gravity anomalies

4.1. Regional gravity patterns

MBA varies significantly in the western Indian Ocean (Fig. 3). The most positive value of MBA in the region, 272 mGal, occurs southeast of the Crozet Plateau (50.83°E, 52.58°S). The Kerguelen Plateau has the lowest MBA value, -321 mGal (at 69.08°E, 48.66°S). Prominent MBA lows are also found in the vicinity of all oceanic plateaus and hotspot features including Tristan, Walvis Ridge, Gough, Discovery, Agulhas Ridge, Agulhas Plateau, Madagascar Ridge, Del Cano Plateau, Crozet Plateau, and Conrad Rise. A broad, irregular low is roughly centered on the BTJ.

All prominent MBA lows persist in the RMBA map (Fig. 5), indicating that these MBA features are not artifacts of lithospheric cooling effects. The most positive RMBA values are found near the RTJ (294 mGal at 58.75°E, 30.67°S), along the AAR (276 mGal at 9.75°W, 57.92°S), and along the Andrew Bain FZ (274 mGal at 30.08°E, 51.25°S). The most negative RMBA values correspond to the Crozet Plateau (-231 mGal

at 50.5°E, 46.2°S) and the Kerguelen Plateau (-294 mGal at 69.08°E, 48.66°S).

4.2. Along-axis gravity

MBA shows pronounced intermediate- to long-wavelength trends along the SWIR (Fig. 3). From west to east, MBA values increase from a regional low at Bouvet Island (-181 mGal) to a high at the Andrew Bain FZ (62 mGal). Similarly, MBA values increase eastward from a regional low near Marion Island (-124 mGal) to a high west of the Melville FZ. An along-axis profile of RMBA shows intermediate- to long-wavelength trends similar to those of MBA (Fig. 5). The lowest RMBA value west of the Andrew Bain FZ occurs near Bouvet Island (26 mGal) while the maximum occurs at ~27°E (195 mGal). To the east, RMBA values generally increase from a low near Marion Island (40 mGal) to a high near the RTJ (~200 mGal).

4.3. Marion

Strict definition of the amplitude and wavelength of the Marion axial gravity anomaly is difficult. Along-axis profiles show short-wavelength variations that are not observed along other hotspot-affected ridges (e.g. the Galapagos spreading center [20]) which may be a function of a number of effects, including the ultra-slow spreading rate, frequent ridge offsets, and relatively sparser data coverage. Broad MBA and RMBA anomalies bracket the central SWIR between the Andrew Bain and Gallieni FZs (Figs. 3 and 5). However, we advocate limiting the Marion plume's eastern boundary to the Discovery II FZ, for several reasons. First, the ridge segment bounded by the dual-offset Discovery II transform faults has locally high MBA. Second, we postulate that the long-offset (350 km) Discovery II transform system is sufficiently long to displace segments to the east out of the range of Marion plume influence, an idea that we develop more thoroughly in a later section. The limited number of shiptrack crossings of SWIR spreading segments near Marion prevents us from assigning an anomaly amplitude.

To the west of Marion, a prominent RMBA high occurs in the vicinity of the Marion and Prince Edward FZs, and further to the west is the pronounced Andrew Bain FZ RMBA high (Fig. 7b). Local surveys of the segments between the Prince Edward and Marion FZs, and the Marion and Andrew Bain FZs, found evidence for extremely robust magmatism, uncharacteristic of slow spreading segments bounded by well-developed transform offsets [10]. It is likely that this robust magmatism is due to the Marion plume. For this reason, we interpret the Marion hotspot axial gravity anomaly to be between the Andrew Bain and Discovery II FZs. This yields an along-axis anomaly of 510 km without counting intervening transform offsets, or 1100 km including the transform faults. Meanwhile we attribute the axial bathymetric high and MBA low between the Indomed and Gallieni FZs to another source. Although the exact cause is unclear at this point, such bathymetric and MBA anomalies could be due to (1) the lack of significant offset in this length of ridge (Fig. 1) and thus less transform cooling effect, (2) remnant effects from the creation of the Del Cano Plateau, or (3) excess volcanism due to another off-axis plume source, such as the Crozet hotspot. However the latter option, linkage to the Crozet hotspot, would require a ridge-hotspot conduit of more than 1000 km from the Crozet Plateau to the SWIR.

Geochemical data, although sparse, also suggest that the Marion effect may be localized. For example, Mahoney et al. [30] noted that the SWIR immediately west of the Prince Edward FZ shows no plume characteristics: it has low $^{87}\text{Sr}/^{86}\text{Sr}$, high $^{143}\text{Nd}/^{144}\text{Nd}$, and low $^{206}\text{Pb}/^{204}\text{Pb}$. In contrast, the segment of ridge between the Prince Edward FZ and the Eric Simpson FZ is distinguished by low Ba/Nb and Zr/Nb, which are characteristics that Mahoney et al. [30] attribute to the Marion plume. These data limit the along-axis length of the geochemical effects of Marion to about 250 km. The adjacent ridge between the Eric Simpson FZ and the Discovery II FZ has high Ba/Nb, low ϵ_{Nd} , high $^{87}\text{Sr}/^{86}\text{Sr}$ and unusually low $^{206}\text{Pb}/^{204}\text{Pb}$. Although Mahoney et al. [30] do not advocate the addition of this length of SWIR to the range of Marion geochemical influence, it is

interesting to note that the spreading centers between the Prince Edward and Discovery II FZs show both pronounced negative RMBA anomalies and anomalous geochemistry. Further geochemical sampling and more shiptrack geophysical data will help to resolve some of the questions surrounding the Marion plume.

4.4. Bouvet

Employing isotope and incompatible element data, le Roex et al. [31,32] find evidence for ba-

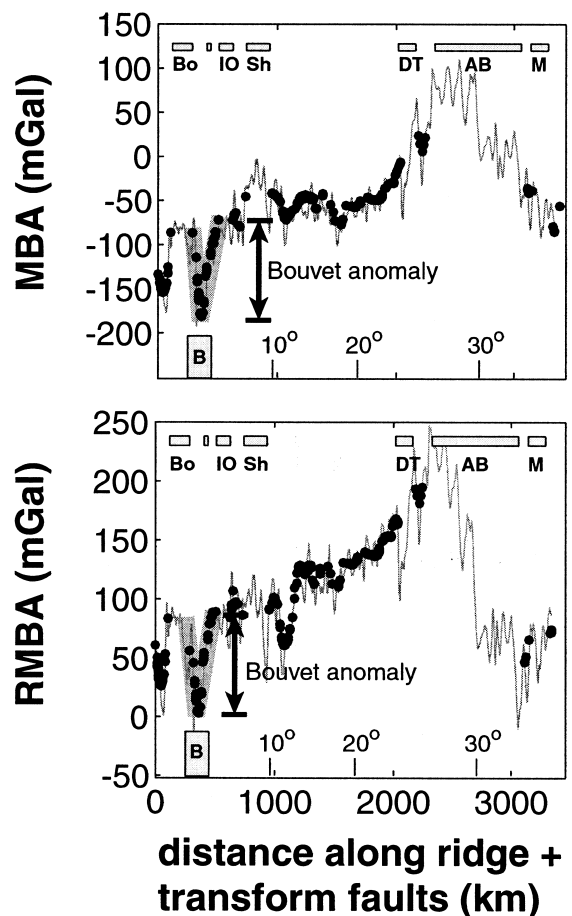


Fig. 7. Along-axis profiles of SWIR MBA and RMBA in the vicinity of the Bouvet plume. As in Figs. 3 and 5, black dots mark the locations constrained by shiptrack crossings of SWIR ridge segments. The location of Bouvet (B) is indicated with a vertical gray bar. Thick, dark gray lines near the Bouvet hotspot indicate the estimated amplitude and wavelength of the plume anomaly.

salts related to the Bouvet hotspot along the SWIR from the BTJ to 14°E. Values of $^{87}\text{Sr}/^{86}\text{Sr}$ and $^{143}\text{Nd}/^{144}\text{Nd}$ are highly scattered from the BTJ to ~14°E, and Zr/Nb data suggest that enriched, transitional, and normal MORB are juxtaposed throughout the length of the affected region. Le Roex et al. [31] and Dick [33] suggested that since the ultra-slow spreading SWIR represents a relatively cold thermal regime, magma chambers along the SWIR are both small and short-lived, allowing the persistence of local geochemical heterogeneities originating from the Bouvet plume.

Gravity calculations, on the other hand, suggest a considerably more localized anomaly. A high-amplitude (~100–125 mGal) MBA low is found between the Bouvet and Islas Orcadas FZs (Fig. 7a), yielding an along-axis distance, excluding transform offsets, of 260 km. Another pronounced MBA low between the BTJ and Bouvet FZ, of ~75–80 mGal amplitude, is associated with Spiess Seamount, possibly also reflecting the Bouvet plume.

A long-wavelength gradient between the Shaka and Andrew Bain FZs is a pronounced feature of the axial RMBA profile (Fig. 7b). However, it is unlikely that this extended gradient should be attributed to Bouvet. Some component of the gradient is attributable to underestimation of the transform effect by the age-based thermal correction method, as compared to the passive upwelling-based method (Fig. 6). More important, limited rock dredging sampling of the section of ridge between 15°E and 25°E shows little or no plume influence [34].

It is interesting to note that there is a high degree of symmetry in plate boundary geometry between the SWIR and the AAR in the vicinity of the BTJ (Fig. 1). The relatively long-offset Bouvet FZ on the SWIR is the conjugate of the Conrad FZ on the AAR, while the Shaka FZ is analogous to the Bullard FZ. Spreading rates along the two ridges are also similar, with a 0.9 cm/yr half-rate for the AAR. In addition, le Roex et al. [35] found a juxtaposition of enriched, transitional, and normal MORB along the AAR to approxi-

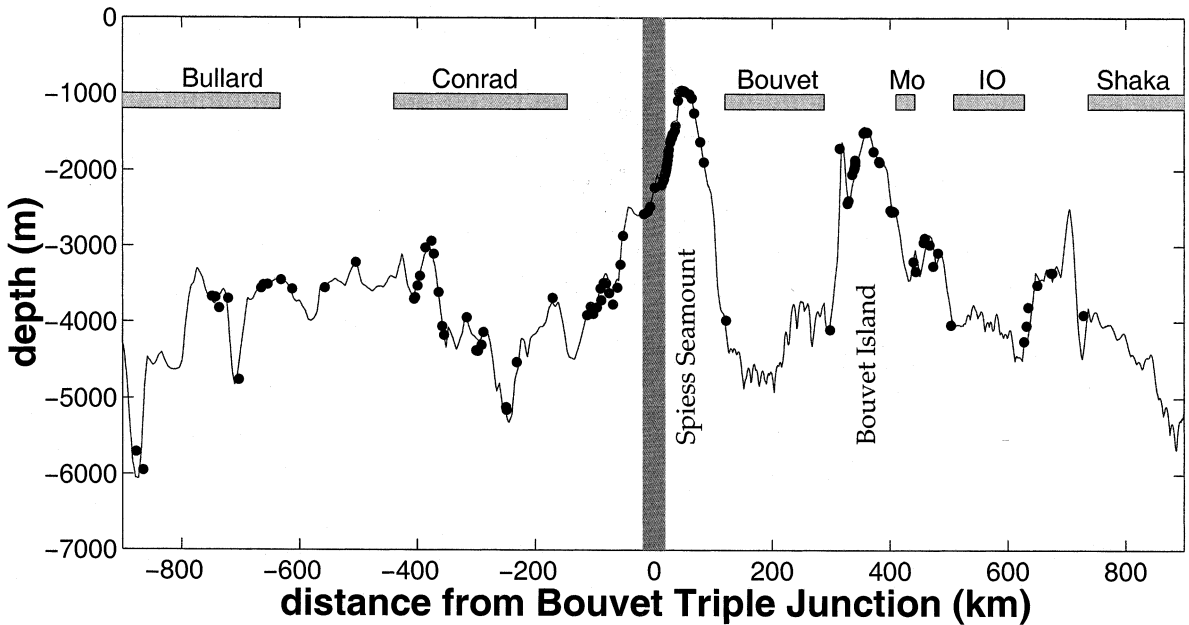


Fig. 8. Axial bathymetric profile along the American–Antarctic (distances < 0 km) and Southwest Indian (distances > 0 km) ridges, from the data source of [2]. Positions of Bullard, Conrad, Bouvet, Moshesh (Mo), Islas Orcadas (IO), and Shaka fracture zones are indicated; BTJ is shown with a vertical gray bar at a distance of 0 km. Black dots show locations where shiptracks cross ridge axes.

mately 18°W. However, although spreading rate, ridge geometry, and geochemistry are similar, bathymetric profiles of the SWIR and AAR are not (Fig. 8). While both ridges show rugged topography, Bouvet Island and Spiess Seamount represent bathymetric anomalies along the SWIR that are not paralleled in the AAR. The geochemical similarity, but bathymetric discrepancy, between the AAR and SWIR may support the notion that geochemical heterogeneity is an inherent feature of south Atlantic mantle, independent of the Bouvet plume source. Another possible explanation of the discrepancy is that complex 3D mantle flow patterns associated with the BTJ may have redistributed the geochemical anomalies represented by the Bouvet plume over a broad area. Geodynamical modeling of upwelling in the vicinity of the BTJ would be necessary to evaluate this mechanism.

5. Hotspot tracks

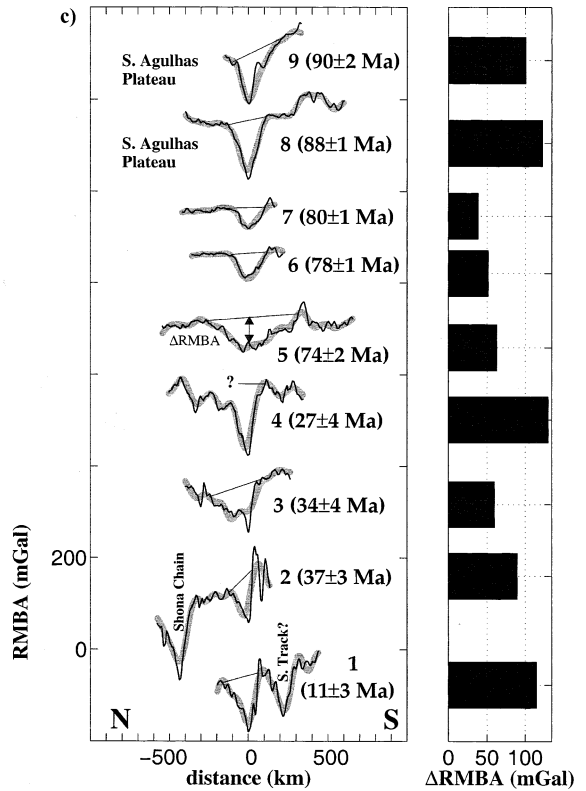
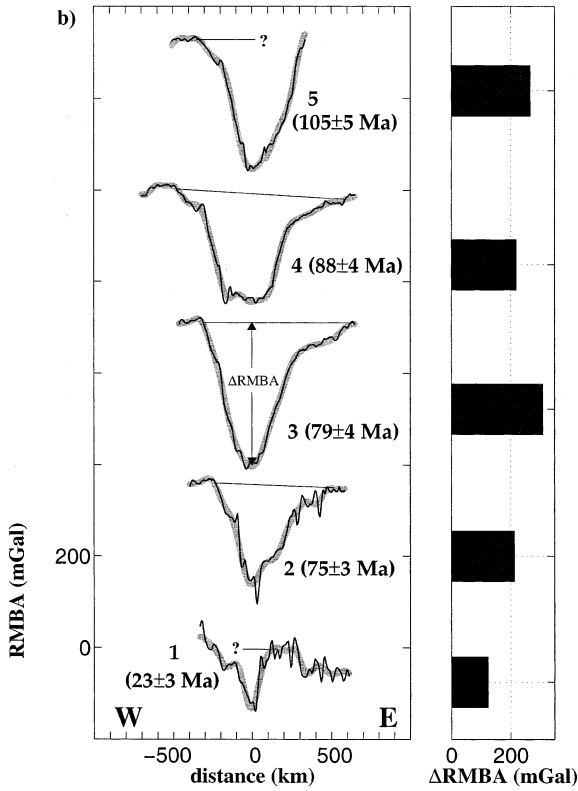
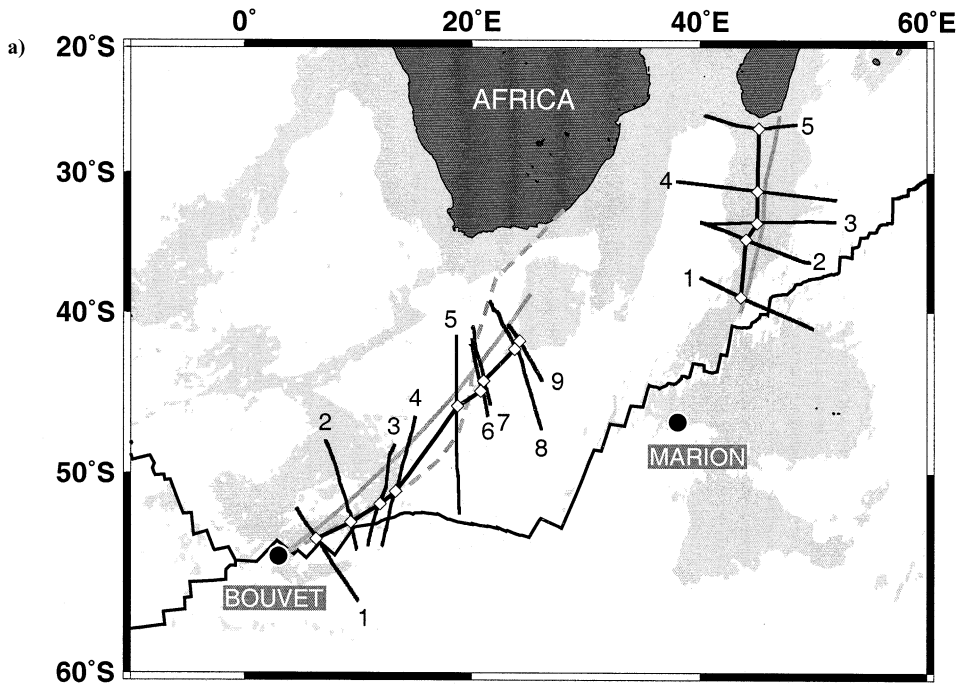
A prominent linear RMBA low extends from Marion Island along the Madagascar Ridge (Figs. 5 and 9a). RMBA profiles taken along shiptracks across this roughly N–S striking low are shown in Fig. 9b. The profiles are aligned so that RMBA minima fall at zero distance. The location of each of these minima is marked on Fig. 9a and connection of the minima forms an off-axis trace of RMBA lows which follow closely the calculated hotspot track for Marion based on the plate reconstruction of Duncan and Richards [36], lending support to the association of thickened crust with hotspot tracks. In general, RMBA

anomaly amplitude is greater for profiles on older crust than younger, which may suggest a decrease in Marion flux over time. However, other explanations are also possible. For example, seismic and gravity studies of the Madagascar Ridge (Fig. 1) suggest it is divided into two provinces, with strongly anomalous crust to the north of 31°S and more normal oceanic crust to the south [37]. Correspondingly, RMBA profiles 4 and 5, to the north of 31°S, are considerably higher amplitude than profiles 1 and 2, both south of 31°S.

Based on a plate reconstruction model of Morgan [5], Hartnady and le Roex [38] presented a solution for the Bouvet hotspot track that extends from southern Africa to the west of the Agulhas Plateau until its intersection with the northeastern Shaka Ridge (Fig. 9a). Hartnady and le Roex [39] also proposed an alternative track based on a single rotation about a 64 Ma pole (Fig. 9a). Connecting the local minima in along shiptrack RMBA yields a line that agrees well with the Morgan-based track for relatively recent times ($< \sim 30$ Ma) and is a little south and east of the Hartnady and le Roex [38] track for earlier periods (Fig. 9a).

Shiptrack RMBA anomaly profiles across the Bouvet track are shown in Fig. 9c. Interestingly, amplitude anomalies are relatively large for profiles 1–4 and 8 and 9, for the most recent and earliest time periods, respectively, but considerably smaller for profiles 5–7 (Fig. 9c). This result confirms Morgan's [5] observation that portions of the Bouvet hotspot track lack bathymetric expression, suggesting at least three possibilities for Bouvet plume history, although other explanations are also possible. First, Bouvet may not rep-

Fig. 9. (a) Simplified map of RMBA, with regions which have RMBA less than 50 mGal shaded gray. The dashed gray line emanating from Bouvet shows a hotspot track calculated by Hartnady and le Roex [38] using finite reconstruction poles from Morgan [5]. The solid gray line from Bouvet shows a track based on rotation about a single, 64 Ma pole [38]. Solid gray line striking roughly N–S is the Marion hotspot track given in Duncan and Richards [36], shifted slightly so zero-age plume location corresponds with Marion Island. Numbered black lines crossing hotspot tracks indicate the locations of RMBA profiles, extracted along shiptrack lines, shown in b and c. Black lines connect local minima in the individual RMBA profiles, with the locations of the local minima shown as white diamonds. (b) Profiles of filtered (thick gray lines) and unfiltered (thin black lines) RMBA along shiptracks crossing the Madagascar Ridge. Profiles are aligned so that local minima fall at roughly zero distance. Crustal ages and age error estimates [3] are provided for each profile, as are thin black lines indicating the definition of Δ RMBA. Δ RMBA amplitudes are shown to the right of the profiles. (c) RMBA profiles along shiptracks to the northeast of Bouvet Island. 'S. Track?' in profile 1 may be a portion of the Bouvet track to the south of the SWIR, resulting from ridge-hotspot interactions. Profiles 8 and 9 cross the southernmost extent of the Agulhas Plateau.



resent a long-lived, deep-seated melting anomaly, but instead a more localized, shallow geochemical heterogeneity tapped relatively recently ($< \sim 30$ Ma) by the SWIR. In this scenario, little or no off-axis expression of the hotspot would be expected. Second, the flux of the Bouvet plume may fluctuate on 10 Myr time scales. Third, it is possible that there is a close relationship between Bouvet plume volcanism and a nearby triple junction. Martin [39] suggests that the paleolocation of the Bouvet plume was coincident with a triple junction at the Agulhas Plateau sometime in the range of 80–100 Ma (Fig. 9c). It may only be through coincidence with a spreading center, or a triple junction and its unusual mantle upwelling patterns, that the weak Bouvet plume develops a bathymetric or gravimetric expression. Further paleomagnetic reconstruction work detailing the position of the triple junction between 90 Ma and the present would be required to examine this possibility more thoroughly.

To the south of the SWIR, a linear RMBA low strikes NW–SE between approximately 3°E and 10°E , roughly mirroring the low anomaly to the north of the ridge (Fig. 5, inset). The easternmost portion of such conjugate lows, at approximately 10°E , may have been created when Bouvet-related volcanism first began along the SWIR (i.e. when the plume first started supplying material to the ridge). Taken together, the northern and southern lows form an RMBA ‘wake’ which converges on the present-day location of the plume, much like the Carnegie and Cocos ridges for the Galapagos plume.

6. Plume–ridge interactions

To examine the effects of ridge offset on ridge–hotspot interactions, we compare the Marion/SWIR and Galapagos/CNSC systems depicted in Fig. 10. These maps, which have the same scale, show that the Marion and Galapagos systems have roughly the same ridge–hotspot separation distance, 250 km and 200 km, respectively. However, the CNSC spreads at more than three times the rate of the SWIR (2.8 cm/yr versus 0.8 cm/yr half-rate, respectively). Further, over the region in

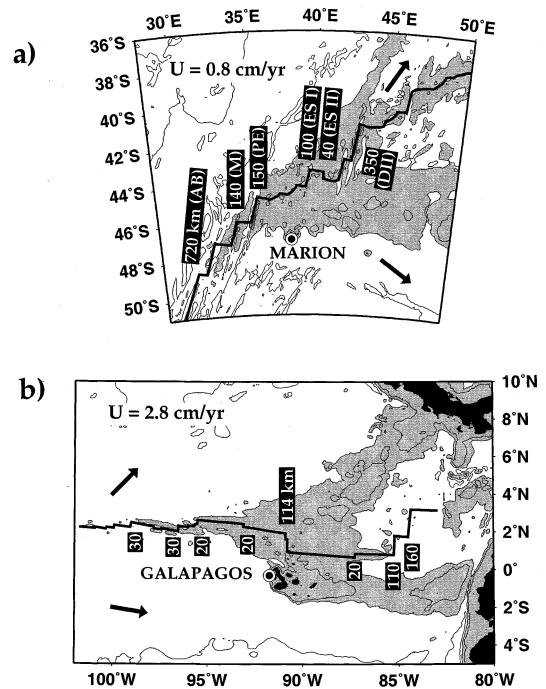


Fig. 10. (a) Bathymetry for the Marion plume region, with depths shallower than 3 km shaded. Selected fracture zones are labeled as in Fig. 1, with transform offsets in km. Arrows indicate absolute plate motion direction [46], U is half-spreading rate, and contours are drawn at 1.5, 3.0, and 4.5 km depth. (b) Bathymetry of the Galapagos archipelago, with depths shallower than 2.75 km shaded. As in (a), selected ridge offset distances are given in km. Contours mark 1.75, 2.75, and 3.75 km depth, and arrows indicate absolute plate motion [46].

Fig. 10, the cumulative ridge offset along the SWIR is 1520 km, again approximately three times the CNSC cumulative offset distance (560 km).

6.1. Plume dispersion along a segmented ridge

Transform offsets may play an important role in ridge–hotspot interactions. Fig. 11 shows two possible scenarios for the ridgeward transport of plume material for ridge geometries that resemble the Galapagos and Marion systems: (1) diffuse plume dispersion (Fig. 11a,b), as suggested by the numerical modeling of Ito et al. [15–17], Ribe [18], and Ribe et al. [19]; and (2) channelized along-axis flow (Fig. 11c,d), following Morgan

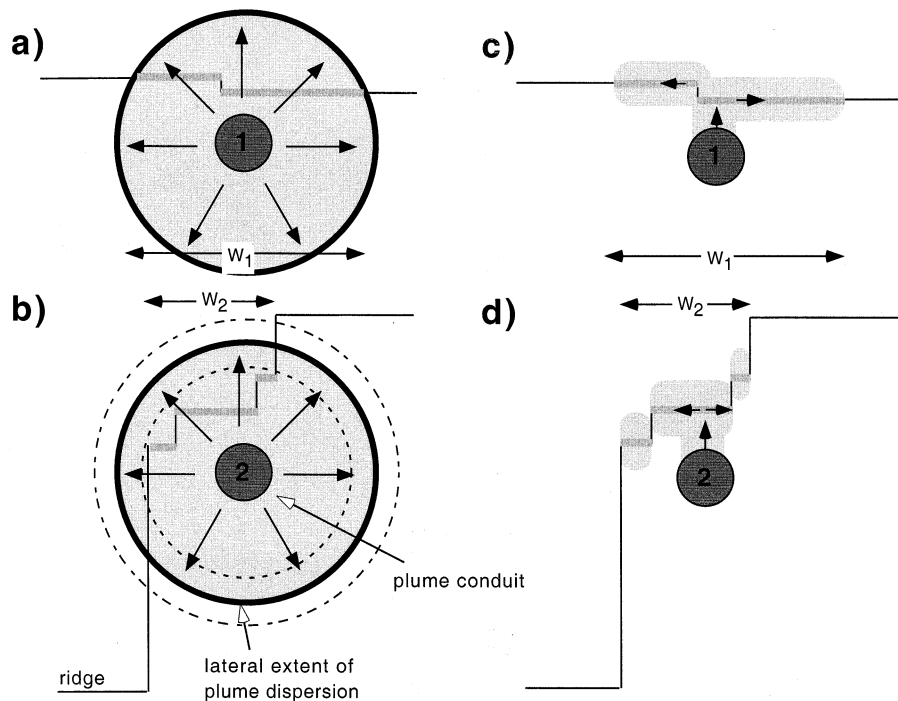


Fig. 11. Schematic cartoons of plume-ridge interaction with a segmented ridge. (a) Broad dispersion of plume material at a depth below the onset of melting, for a ridge with only a single, small transform offset. Dark gray circle represents the plume conduit, light gray shading depicts dispersal of plume material, arrows indicate plume dispersal direction, and thin black lines denote ridge geometry. Ridge segments with a plume signature are emphasized with thick, medium gray shading. The length of ridge affected by plume 1, or waist width, is W_1 . (b) As in (a), but for a highly segmented ridge. Although the plume's lateral extent is the same as in (a), the resulting waist width W_2 is less than W_1 . Note ambiguity in inferring plume dispersion from W_2 , since both smaller (dashed) and larger (dash-dot) circles will produce the same W_2 . (c) Schematic illustration of the channelized along-axis plume dispersion model for the same ridge geometry as in (a). Arrows indicate flow directed from plume to ridge, and subsequent dispersion along-axis, at depths within the partial melting zone. The resulting waist width is W_1 . (d) As for (c), but for a highly segmented ridge. Note that long-offset transforms act as thermal and mechanical barriers and prevent along-axis dispersion, resulting in a W_2 that is less than W_1 .

[40], Vogt and Johnson [41], Vogt [42], and Sleep [43]. In the scenario of diffuse flow (Fig. 11a,b), a plume upwells vertically to a depth below the region of partial melting, and then spreads radially. The style of plume-ridge interaction will differ depending on ridge-transform geometry. If the ridge offset is small (Fig. 11a), the plume waist width will reflect well the width of the plume anomaly. For highly segmented geometry (Fig. 11b), however, transform faults offset the ridge out of the area of plume influence, thereby decreasing the waist width. The true lateral extent and flux of the plume will be ambiguous, because plumes with a somewhat smaller or larger areal extent will result in the same waist width.

In the other end-member geometry of channelized along-axis flow (Fig. 11c,d), mantle flows directly from plume to ridge, with subsequent along-axis distribution within or above the melting zone. Here, transform offsets may act as thermal and mechanical barriers to along-axis plume dispersion. Longer offsets compartmentalize hotspot material more effectively than shorter discontinuities. In this case, the plume waist width is also related to ridge geometry, with waist width for a more segmented ridge always less than or equal to that of a straight ridge. Importantly, therefore, both the diffuse dispersion and channelized along-axis flow models imply that ridge segmentation acts to decrease plume waist width.

6.2. Marion and Galapagos

The present paucity of geophysical and geochemical data for the Marion region, and particularly the lack of seismic data, makes it difficult to distinguish between the diffuse and channelized plume dispersion models. Here we note that two prominent transform faults disrupt the SWIR in the vicinity of Marion, Andrew Bain (total offset of 720 km) and Discovery II (total offset of 350 km) (Fig. 10a). These transforms appear to bracket the along-axis MBA and RMBA anomalies for Marion (Figs. 3 and 5). Therefore, we postulate that these two transform systems are long enough to limit Marion's waist width, or to act as 'transform terminators'. We do not presently have enough data to conclusively determine if Andrew Bain and Discovery II limit Marion's waist width by offsetting the SWIR out of Marion's influence (diffuse plume model) or damming along-axis flow (channelized plume model).

In contrast to Marion, there are few significant ridge discontinuities along the CNSC near the Galapagos (Fig. 10b). No discontinuities greater than 35 km exist to the west of the Galapagos Islands, suggesting that the western half-width of the Galapagos anomaly reflects the original plume width. The eastern CNSC also has few discontinuities between the Galapagos Islands and $\sim 85^\circ\text{W}$; however, a 110-km transform at 85°W may terminate the Galapagos anomaly. Taken together, the Marion/SWIR and Galapagos/CNSC examples illustrate the important influence of transform offsets in limiting the lateral extent of plume–ridge interaction at a variety of spreading rates. Since ultra-slow spreading ridges tend to be more highly segmented, the transform effect may be most pronounced along the SWIR. The effects of transform offset length and spreading rate on along-axis flow from a ridge-centered plume are quantitatively evaluated through numerical modeling in a separate study [44].

7. Conclusions

The main results of this study of ridge–hotspot

interactions along the SWIR include the following:

1. The Bouvet hotspot, approximately 300 km east of the BTJ and 55 km from the nearest spreading segment along the SWIR, imparts a high-amplitude (~ 100 mGal) mantle Bouguer gravity anomaly low to the SWIR, implying considerable crustal thickening, anomalously warm mantle, or a combination of both. However, the Bouvet anomaly is quite localized between the Bouvet and Islas Orcadas FZs. In comparison, the Marion MBA low is broader, and likely limited to the stretch of ridge between the Andrew Bain and Discovery II FZs.
2. There is little off-axis indication of a Bouvet hotspot track in crust ~ 30 – 90 Ma, suggesting the possibilities that the flux of the hotspot changes with time, or that the hotspot melting anomaly is enhanced when it is close to a plate boundary. In contrast, a well-defined residual gravity low, striking north–south along the Madagascar Ridge, corresponds closely with published Marion hotspot tracks.
3. Long-offset transforms, characteristic of ultra-slow spreading centers, may play an important role in influencing ridge–hotspot interactions. Transforms may either act as thermal and mechanical barriers to along-axis plume transport, or displace ridge segments out of a hotspot-affected region. We postulate that the Andrew Bain and Discovery II FZs, with offsets of 720 and 350 km, respectively, act as 'transform terminators' for the Marion plume.

Acknowledgements

We are grateful to R. Fisher, J. Sclater, and A. Goodwillie for providing the GEBCO-97 bathymetric data of the southern oceans and to J. Madson, N. Grindlay, C. Rommevaux-Jestin, and M. Cannat for providing reprints of their manuscripts. Constructive reviews by Roger Searle and an anonymous reviewer improved the manuscript. We benefited greatly from discussion with M. Cannat, B. Detrick, J. Escartin, G. Ito, and B.

West. This work was supported by a National Defense Science and Engineering Graduate (NDSEG) Fellowship to J.G. and NSF Grants OCE-9811924 and OCE-9907630. Woods Hole Oceanographic Institution contribution number 10311. [FA]

References

- [1] D.T. Sandwell, W.H.F. Smith, Marine gravity anomaly from Geosat and ERS 1 satellite altimetry, *J. Geophys. Res.* 102 (1997) 10039–10054.
- [2] IOC, IHO, and BODC, GEBCO-97: The 1997 Edition of the GEBCO Digital Atlas, 1997.
- [3] R.D. Mueller, W.R. Roest, J.-Y. Royer, L.M. Gahagan, J.G. Sclater, Digital isochrons of the world's ocean floor, *J. Geophys. Res.* 102 (1997) 3211–3214.
- [4] R.A. Duncan, Hotspots in the southern oceans – an absolute frame of reference for motion of the Gondwana continents, *Tectonophysics* 74 (1981) 29–42.
- [5] W.J. Morgan, Hotspot tracks and the early rifting of the Atlantic, *Tectonophysics* 94 (1982) 123–139.
- [6] M. Ligi, E. Bonatti, G. Bortoluzzi, G. Carrara, P. Fabbretti, D. Penitenti, D. Gilod, A.A. Peyve, S. Skolotnev, N. Turko, Death and transfiguration of a triple junction in the south Atlantic, *Science* 276 (1997) 243–245.
- [7] M.D. Kurz, A.P. leRoex, H.J.B. Dick, Isotope geochemistry of the oceanic mantle near the Bouvet triple junction, *Geochim. Cosmochim. Acta* 62 (1998) 841–852.
- [8] N.C. Mitchell, R.A. Livermore, Spiess Ridge: An axial high on the slow spreading Southwest Indian Ridge, *J. Geophys. Res.* 103 (1998) 15457–15471.
- [9] N.R. Grindlay, J. Madsen, C. Rommevaux-Jestin, J. Sclater, A different pattern of ridge segmentation and mantle Bouguer gravity anomalies along the ultra-slow spreading Southwest Indian Ridge (15°30'E to 25°E), *Earth Planet. Sci. Lett.* 161 (1998) 243–253.
- [10] N.R. Grindlay, J. Madsen, C. Rommevaux, J. Sclater, S. Murphy, Southwest Indian Ridge 15°E–35°E: A geophysical investigation of an ultra-slow spreading mid-ocean ridge system, *InterRidge News* 5 (1996) 7–12.
- [11] P. Patriat, D. Sauter, M. Munsch, L. Parson, A survey of the Southwest Indian Ridge axis between Atlantis II Fracture Zone and the Indian Ocean Triple Junction: Regional setting and large scale segmentation, *Mar. Geophys. Res.* 19 (1997) 457–480.
- [12] C. Rommevaux-Jestin, C. Deplus, P. Patriat, Mantle Bouguer anomaly along an ultra-slow spreading ridge: Implications for accretionary processes and comparison with results from central Mid-Atlantic Ridge, *Mar. Geophys. Res.* 19 (1997) 481–503.
- [13] C. Mevel, K. Tamaki, The FUJI scientific party, Imaging an ultra-slow spreading ridge: first results of the FUJI cruise on the SWIR (R/V Marion Dufresne, 7/10–3/11/97), *InterRidge News* 7 (1998) 29–32.
- [14] M. Cannat, C. Rommevaux-Jestin, D. Sauter, C. Deplus, V. Mendel, Formation of the axial relief at the very slow spreading Southwest Indian Ridge (49 degrees to 69 degrees E), *J. Geophys. Res.* 104 (1999) 22825–22843.
- [15] G. Ito, J. Lin, C.W. Gable, Dynamics of mantle flow and melting at a ridge-centered hotspot: Iceland and the Mid-Atlantic Ridge, *Earth Planet. Sci. Lett.* 144 (1996) 53–74.
- [16] G. Ito, J. Lin, C.W. Gable, Interaction of mantle plumes and migrating mid-ocean ridges: Implications for the Galapagos plume–ridge system, *J. Geophys. Res.* 102 (1997) 15403–15417.
- [17] G. Ito, Y. Shen, G. Hirth, C.J. Wolfe, Mantle flow, melting, and dehydration of the Iceland mantle plume, *Earth Planet. Sci. Lett.* 165 (1999) 81–96.
- [18] N.M. Ribe, U.R. Christensen, J. Theißing, The dynamics of plume–ridge interaction, 1: Ridge-centered plumes, *Earth Planet. Sci. Lett.* 134 (1995) 155–168.
- [19] N.M. Ribe, The dynamics of plume–ridge interaction, 2: Off-ridge plumes, *J. Geophys. Res.* 101 (1996) 16024–16195.
- [20] G. Ito, J. Lin, Mantle temperature anomalies along the present and paleoaxes of the Galapagos spreading center as inferred from gravity analysis, *J. Geophys. Res.* 100 (1995) 3733–3745.
- [21] B. Appelgate, A.N. Shor, The northern Mid-Atlantic and Reykjanes Ridges: Spreading center morphology between 55°50'N and 63°00'N, *J. Geophys. Res.* 99 (1994) 17935–17956.
- [22] R.L. Fisher, A.M. Goodwillie, The physiography of the Southwest Indian Ridge, *Mar. Geophys. Res.* 19 (1997) 451–455.
- [23] G.A. Neumann, D.W. Forsyth, D. Sandwell, Comparison of marine gravity from shipboard and high-density satellite altimetry along the Mid-Atlantic Ridge, 30.5°–35.5°S, *Geophys. Res. Lett.* 20 (1993) 1639–1642.
- [24] D. Divens, Total sediment thickness of the world's oceans, National Oceanic and Atmospheric Administration, US Department of Commerce, Boulder, CO, 1996 (information available on the Web at <http://www.ngdc.noaa.gov/mgg/sedthick/sedthick.html>).
- [25] B. Parsons, J.G. Sclater, An analysis of the variation of ocean floor bathymetry and heat flow with age, *J. Geophys. Res.* 82 (1977) 803–827.
- [26] D.L. Turcotte, E.R. Oxburgh, Finite amplitude convection cells and continental drift, *J. Fluid Mech.* 28 (1967) 29–42.
- [27] B.Y. Kuo, D.W. Forsyth, Gravity anomalies of the ridge-transform system in the South Atlantic between 31 and 34.5°S: Upwelling centers and variations in crustal thickness, *Mar. Geophys. Res.* 10 (1988) 205–232.
- [28] J. Lin, G.M. Purdy, H. Schouten, J.-C. Sempere, C. Zervas, Evidence from gravity data for focused magmatic accretion along the Mid-Atlantic Ridge, *Nature* 344 (1990) 627–632.
- [29] J. Phipps Morgan, D.W. Forsyth, 3-D flow and temper-

- ature perturbations due to transform offset: effects on oceanic crustal and upper mantle structure, *J. Geophys. Res.* 93 (1988) 2955–2966.
- [30] J. Mahoney, A.P. le Roex, Z. Peng, R.L. Fisher, J.H. Natland, Southwestern limits of Indian Ocean ridge mantle and the origin of low $^{206}\text{Pb}/^{204}\text{Pb}$ mid-ocean ridge basalt: Isotope systematics of the central Southwest Indian Ridge (17°–50°E), *J. Geophys. Res.* 97 (1992) 19771–19790.
- [31] A.P. le Roex, H.J.B. Dick, A.J. Erlank, A.M. Reid, F.A. Frey, S.R. Hart, Geochemistry, mineralogy and petrogenesis of lavas erupted along the Southwest Indian Ridge between the Bouvet Triple Junction and 11 degrees east, *J. Petrol.* 24 (1983) 267–318.
- [32] A.P. le Roex, H.J.B. Dick, R.T. Watkins, Petrogenesis of anomalous K-enriched MORB from the Southwest Indian Ridge: 11°53'E to 14°38'E, *Contrib. Mineral. Petrol.* 110 (1992) 253–268.
- [33] H.J.B. Dick, Abyssal peridotites, very slow spreading ridges, and ocean ridge magmatism, in: A.D. Saunders, M.J. Norry (Eds.), *Magmatism in the Ocean Basins*, Geological Society special publication No. 42, 1989, pp. 71–105.
- [34] H.J.B. Dick, A.P. leRoex, J. Madsen, N.R. Grindlay, Constraints on mantle melting, diapirism and melt flow at ultra-slow spreading ridges: observations from petrological and geophysical data from the Southwest Indian Ridge 15 to 25 degrees east, *EOS Trans. AGU* 78 (Suppl.) (1997) F682–F683.
- [35] A.P. le Roex, H.J.B. Dick, A.M. Reid, F.A. Frey, A.J. Erlank, S.R. Hart, Petrology and geochemistry of basalts from the American–Antarctic Ridge, Southern Ocean: Implications for the westward influence of the Bouvet mantle plume, *Contrib. Mineral. Petrol.* 90 (1985) 367–380.
- [36] R.A. Duncan, M.A. Richards, Hotspots, mantle plumes, flood basalts, and true polar wander, *Rev. Geophys.* 29 (1991) 31–50.
- [37] J. Goslin, M. Recq, R. Schlich, Structure profonde du plateau de Madagascar: relations avec le plateau de Crozet, *Tectonophysics* 76 (1981) 75–97.
- [38] C.J.H. Hartnady, A.P. le Roex, Southern Ocean hotspot tracks and the Cenozoic absolute motion of the African, Antarctic, and South American plates, *Earth Planet. Sci. Lett.* 75 (1985) 245–257.
- [39] A.K. Martin, Plate reorganisations around Southern Africa, hot-spots and extinctions, *Tectonophysics* 147 (1987) 309–316.
- [40] W.J. Morgan, Rodriguez, Darwin, Amsterdam, ..., A second type of hotspot island, *J. Geophys. Res.* 83 (1978) 5355–5360.
- [41] P.R. Vogt, G.L. Johnson, Transform faults and longitudinal flow below the midoceanic ridge, *J. Geophys. Res.* 80 (1975) 1399–1428.
- [42] P.R. Vogt, Plumes, subaxial pipe flow, and topography along the mid-oceanic ridge, *Earth Planet. Sci. Lett.* 29 (1976) 309–325.
- [43] N. Sleep, Lateral flow of plume material ponded at sublithospheric depths, *J. Geophys. Res.* 101 (1996) 28065–28083.
- [44] J. Georgen, J. Lin, The effects of transform offsets on reducing along-ridge plume flux: Implications for ridge–hotspot interactions, *EOS Trans. AGU* 81 (Suppl.) (2000) F1129.
- [45] R.L. Parker, The rapid calculation of potential anomalies, *Geophys. J. R. Astron. Soc.* 31 (1972) 447–455.
- [46] A.E. Gripp, R.G. Gordon, Current plate velocities relative to the hotspots incorporating the NUVEL-1 global plate motion model, *Geophys. Res. Lett.* 17 (1990) 1109–1112.